Investigating receptor enzyme activity using time scale analysis

Tao You[1], Hong Yue[2]

[1]Computational Biology, Discovery Sciences, Innovative Medicines & Early Development, AstraZeneca, Alderley Park, Cheshire, SK10 4TG, UK. Email: dr.tao.you@gmail.com

[2]Department of Electrical and Electronic Engineering, University of Strathclyde, Glasgow, G1 1XW, UK. Email: hong.yue@strath.ac.uk

Abstract

At early drug discovery, purified protein-based assays are often used to characterize compound potency. In the context of dose response, it is often perceived that a time-independent inhibitor is reversible and a time-dependent inhibitor is irreversible. The legitimacy of this argument is investigated using a simple kinetics model, where it is revealed by model-based analytical analysis and numerical studies that dose response of an irreversible inhibitor may appear time-independent under certain parametric conditions. Hence, the observation of time-independence cannot be used as sole evidence for identification of inhibitor reversibility. It has also been discussed how the synthesis and degradation of a target receptor affect drug inhibition in an *in vitro* cell-based assay setting. These processes may also influence dose response of an irreversible inhibitor in such a way that it appears time-independent under certain conditions. Furthermore, model-based steady-state analysis reveals the complexity nature of the drug-receptor process.

Keywords

Inhibitor reversibility; receptor turnover; mathematical modelling; dose response; time-scale analysis

1 Introduction

Drug discovery and development typically involve protein-based studies (e.g. target engagement; typical time scale: microseconds to minutes), *in vitro* cell-based studies (e.g. biomarker pharmacodynamics (PD), therapeutic efficacy; typical time scale: minutes to days), *in vivo* animal-based studies (e.g. pharmacokinetics (PK), biomarker PD, therapeutic efficacy, safety evaluation; typical time scale: hours to days) and clinical trials (e.g. PK, PD, safety, efficacy; typical time scale: days to months). These studies are often organized in this particular temporal order, in the hope that the results of a previous step (e.g. protein-based assay) will help inform the design and interpretation of the subsequent experiment (e.g. *in vitro* cell assay).

A new paradigm that helps enable robust translation of each type of study arises in recent years [1], in which mathematical models and model-based systems analysis have played increasingly important roles. Model development of drug processes using experimental data has been largely improved through various efforts including sensitivity analysis, parameter identifiability analysis, model approximation and simplification, model validation and comparison, etc. [2-5].

Known as Quantitative & Systems Pharmacology (QSP), it employs multi-scale modelling approaches to integrate data generated from different studies in a drug discovery and development programme, which span different temporal and dimensional scales [6-8]. These computational models are able to reconcile different experimental conditions (e.g. *in vitro* cell assays and *in vivo* animal models [9]), with an ultimate aim of bridging preclinical models to an appropriate clinical setting, and generating statistically robust predictions that are validated by preclinical and clinical data [10].

Multi-scale modelling has been successfully deployed in drug development programmes, so that *in vitro* cell-based studies are consistently integrated with *in vivo* animal-based studies. However, the application of QSP approaches in early drug discovery (i.e. integration of results from protein-based studies and *in vitro* cell-based studies) has been relatively limited [11]. QSP models are urgently needed to better understand target engagement in cell-free environment and in cells, so as to help design of subsequent *in vitro* and *in vivo* studies [1].

It is often important to establish dose–response relationship specific for an inhibitor and a cell type under investigation, which describes the change in effect on a cell caused by differing levels of exposure (or doses) to an inhibitor after a certain exposure time.

To help translate *in vitro* results into *in vivo* knowledge, models of Target Mediated Drug Disposition (TMDD) have been developed to analyse receptor PK/PD relationships [2-5; 7; 8; 12-15]. In addition to drug binding and receptor turnover, these models also consider the elimination of all species, to mimic *in vivo* conditions. They can be served as a useful theoretical framework. Model-based analysis revealed that the necessary and sufficient condition for receptor rebound in a single dose animal experiment is that elimination rate of the drug-receptor product being slower than the elimination rates of the drug and of the receptor [12]. Under the assumption of a constant target pool, the characteristic features of TMDD dynamics were studied through a mathematical model analysis [13]. A time-scale analysis was performed to provide accurate approximations of the temporal evolution under the assumption of high drug binding affinity [14].

Although TMDD models have been used increasingly to facilitate PK/PD studies, cellular kinetics may sometimes not be fully appreciated in design of protein-based assays. For instance, the potency of a chemical entity to inhibit an enzyme is often characterized by IC_{50}, the chemical concentration that generates half of maximal inhibition. For an irreversible inhibitor that covalently modifies a purified target enzyme in a cell-free assay, the chemical reaction tends to be more complete given a longer drug incubation period. Consequently, IC_{50} usually exhibits incubation time-dependent shift, making the inhibitor appear more potent at long incubation periods [16-18]. In contrast, a target protein in a living cell undergoes turnover (i.e. synthesis and degradation) that are often regulated via transcriptional regulation, translational control [19] and cell signalling etc. These processes typically happen within minutes to hours [20], and they may influence cellular response to drug inhibition. In other words, shooting a moving target in a cell might be different from shooting an immobile target in a protein-based assay.

The aim of this study is to investigate how drug parameters and cell parameters influence cellular response to drug treatment at constant drug concentration. We are interested in understanding whether an irreversible inhibitor necessarily has an incubation time-dependent IC_{50} in a protein-based study. In addition, we hope to examine how cell parameters including target synthesis and degradation rates affect dose response.

The remaining of the paper is organized as follows. A linear model of receptor turnover and irreversible inhibition is proposed and discussed in Section 2. Investigation of fast drug process relative to receptor turnover is discussed in Section 3, where both numerical simulation and ensuing analysis of the eigenvalues are employed. Discussions on slow drug

process relative to receptor turnover are presented in Section 4. In Section 5, an application of this model is attempted using aberrant activity in Epidermal Growth Factor Receptor (EGFR) signaling data. Conclusions are given in Section 6.

2 A model of receptor turnover and drug inhibition

A simple model is proposed to recapitulate the process of receptor turnover, i.e. receptor synthesis and degradation, together with drug inhibition as shown schematically in Fig. 1.

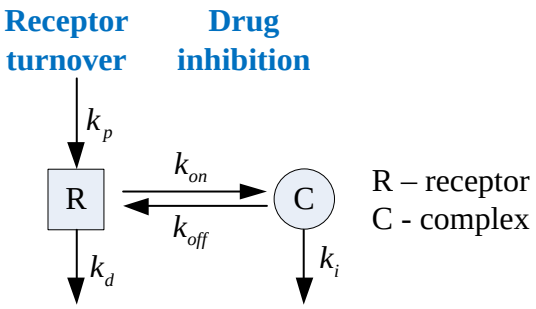

Fig. 1 Schematic description of receptor turnover and irreversible inhibition

In the receptor turnover process, receptor R is synthesized at a constant rate k_p, and degrades following a first-order kinetics with a rate constant k_d. For the sake of simplicity, feedback mechanisms and subcellular localisation that regulate protein synthesis and stability are not considered in this model. In the drug inhibition process, a drug molecule first binds R reversibly to comprise an intermediate complex C with association and dissociation rates k_{on} and k_{off}, respectively. Note that k_{on} is an apparent rate that depends on drug concentration. The complex C then forms a covalent bound irreversibly at the second step, in a first-order reaction with a rate constant k_i. These two processes can be described respectively as follows.

$$\text{Receptor turnover:} \quad \xrightarrow{k_p} \text{R} \xrightarrow{k_d} \tag{1}$$

$$\text{Drug inhibition:} \quad \text{R} \underset{k_{off}}{\overset{k_{on}}{\rightleftharpoons}} \text{C} \xrightarrow{k_i} \tag{2}$$

Based on mass-balance principles, the corresponding ordinary differential equations (ODEs) for concentrations of R and C, denoted as *R* and *C*, respectively, are written as

$$\frac{\mathrm{d}R}{\mathrm{d}t} = -\left(k_d + k_{on}\right)R + k_p + k_{off}C \tag{3}$$

$$\frac{\mathrm{d}C}{\mathrm{d}t} = k_{on}R - \left(k_{off} + k_i\right)C \tag{4}$$

with the following units: nM for *R*, *C*; nM·min^{-1} for k_p; and min^{-1} for k_d, k_{on}, k_{off} and k_i. Here k_p and k_d are cell parameters associated to receptor turnover; k_{on}, k_{off} and k_i are drug parameters for covalent inhibition process.

In the absence of drug, the receptor has a steady state at $R_0 = k_p/k_d$ nM. Scaling *R* and *C* with R_0 in (3) and (4), the two concentration variables become dimensionless terms $r = R/R_0 = Rk_d/k_p$ and $c = C/R_0 = Ck_d/k_p$, respectively, and the ODE model can then be written as

$$\frac{\mathrm{d}r}{\mathrm{d}t} = -\left(k_d + k_{on}\right)r + k_d + k_{off}c \tag{5}$$

$$\frac{\mathrm{d}c}{\mathrm{d}t} = k_{on}r - \left(k_{off} + k_i\right)c \tag{6}$$

In this dimension-free representation, the initial conditions are set to be $r_0 = r(0) = 1$ and $c_0 = c(0) = 0$. We further use k_{off} to scale the time term by $\tau = k_{off}t$, and also to scale reaction rates with $\kappa_{on} = k_{on}/k_{off}$, $\kappa_i = k_i/k_{off}$, and $\kappa_d = k_d/k_{off}$. This brings the following two ODEs for dimensionless *r* and *c*, respectively:

$$\frac{\mathrm{d}r}{\mathrm{d}\tau} = -\left(\kappa_{on} + \kappa_d\right)r + c + \kappa_d \tag{7}$$

$$\frac{\mathrm{d}c}{\mathrm{d}\tau} = \kappa_{on}r - \left(1 + \kappa_i\right)c \tag{8}$$

Denoting $\mathbf{X} = \begin{bmatrix} r & c \end{bmatrix}^{\mathrm{T}}$, this ODE model can be written in a matrix format

$$\dot{\mathbf{X}} = \begin{bmatrix} \dot{r} \\ \dot{c} \end{bmatrix} = \begin{bmatrix} \dfrac{\mathrm{d}r}{\mathrm{d}\tau} \\ \dfrac{\mathrm{d}c}{\mathrm{d}\tau} \end{bmatrix} = \begin{bmatrix} -\left(\kappa_{on} + \kappa_d\right) & 1 \\ \kappa_{on} & -\left(1 + \kappa_i\right) \end{bmatrix} \begin{bmatrix} r \\ c \end{bmatrix} + \begin{bmatrix} \kappa_d \\ 0 \end{bmatrix} \tag{9}$$
$$= \mathbf{AX} + \mathbf{f} \qquad \text{with} \qquad \mathbf{X}(0) = \mathbf{X}_0$$

where $\mathbf{A}=\begin{bmatrix}-(\kappa_{on}+\kappa_d) & 1\\ \kappa_{on} & -(1+\kappa_i)\end{bmatrix}$ is the state matrix for this linear-time-invariant (LTI) system; $\mathbf{f}=\begin{bmatrix}\kappa_d & 0\end{bmatrix}^{\mathrm{T}}$ is the nonhomogeneous part; $\mathbf{X}_0=\begin{bmatrix}1 & 0\end{bmatrix}^{\mathrm{T}}$ is the vector of initial states for **X**.

At the steady state when $\mathrm{d}r/\mathrm{d}\tau=0$ and $\mathrm{d}c/\mathrm{d}\tau=0$, the steady-state values for r and c are derived from (9) to give

$$r_{ss}=\frac{(1+\kappa_i)\kappa_d}{(1+\kappa_i)\kappa_d+\kappa_{on}\kappa_i} \tag{10}$$

$$c_{ss}=\frac{\kappa_{on}\kappa_d}{(1+\kappa_i)\kappa_d+\kappa_{on}\kappa_i} \tag{11}$$

Here r_{ss} and c_{ss} are used to denote steady-state values or equilibrium points for r and c, respectively, when time approaches infinity.

Note after the above re-scaling, all terms in (9) are dimensionless including concentration variables r and c; time τ; and parameters κ_{on}, κ_i, and κ_d. The 'disappeared' receptor synthesis rate k_p is included in κ_d through scaling of $\kappa_d=k_d/k_{off}=k_p/(k_{off}R_0)$. Clearly this choice of non-dimensionalization requires that $k_{off}\neq 0$ and $k_p\neq 0$. All variables and parameters in (9) are associated with physical quantities and therefore must be nonnegative. With this dimensionless model, the analysis of system behaviour under different parametric regimes can be conveniently discussed in a unified scheme.

3 Fast drug process relative to receptor turnover

The parametric regimes have been divided into that of fast drug process and slow drug process. In this section, the process of fast drug binding and dissociation is firstly discussed.

3.1 Fast drug binding and dissociation relative to receptor turnover

This parametric regime is defined by $k_{off}\gg k_d$ and $k_{on}\gg k_d$. In this case, the receptor turnover rate k_d is much smaller than the drug binding and dissociation rates k_{on} and k_{off}.

(a) When $k_{off} \gg k_d$, i.e., $\kappa_d \ll 1$, the period of target coverage (characterized by $1/k_{off}$) is much shorter than that of receptor degradation (characterized by $1/k_d$), which can be due to: i) short target coverage; ii) slow receptor degradation; and iii) combination of i) and ii).

(b) When $k_{on} \gg k_d$, i.e., $\kappa_{on} \gg \kappa_d$, a receptor binds a drug molecule at a rate much faster than its degradation.

Under these two conditions, the term of κ_d can be ignored, and model (9) is approximated by

$$\begin{bmatrix} \dot{r} \\ \dot{c} \end{bmatrix} = \begin{bmatrix} -\kappa_{on} & 1 \\ \kappa_{on} & -(1+\kappa_i) \end{bmatrix} \begin{bmatrix} r \\ c \end{bmatrix} \tag{12}$$

Model (12) is actually an ODE model for the cell-free assay with only the drug process in (2) considered.

When $\kappa_i \neq 0$, by taking $\mathrm{d}r/\mathrm{d}\tau = 0$ and $\mathrm{d}c/\mathrm{d}\tau = 0$, the steady-state of dynamic system (12) is deduced to be

$$r_{ss} = c_{ss} = 0 \tag{13}$$

How small does k_d have to be in comparison to k_{off} and k_{on} so as to ensure the validity of this approximation? This is examined by the following numerical simulation. Firstly, the full model in (9) is simulated with $\kappa_i = 0.001$ ($k_{off} \gg k_i$) at three different levels of κ_d: $\kappa_d = 10^{-4}$ (Fig. 2 (a)); $\kappa_d = 10^{-6}$ (Fig. 2 (b)); and $\kappa_d = 10^{-8}$ (Fig. 2 (c)). Then the full model is simulated by taking $\kappa_d = 0$, which is equivalent to the reduced model in (12), using identical value for κ_i, as shown in Fig. 2 (d). The range of κ_{on} is set to be [1e-5, 1e5] in all simulations. Four incubation time periods are chosen which are separated with an order of 3 in time scale between each two, i.e., 10^{-3}, 1, 10^3 and 10^6. Comparing simulation results across the four panels in the semi-log Fig. 2, it can be observed that there is a clear difference in dose response in both Fig. 2 (a) and Fig. 2 (b) when compared with the simplified model results in Fig. 2 (d), but the dose response in Fig. 2 (c) is almost the same as that in Fig. 2 (d). This shows that, when $\kappa_d \leq 10^{-8}$, model (12) provides a close approximation for dose responses corresponding to incubation time up to 10^6.

In all simulation and illustrative results in this paper, the time terms are represented in τ (time t scaled by k_{off}), and the x-axis for κ_{on} is in $\log_{10}$ scale in dose-response curves.

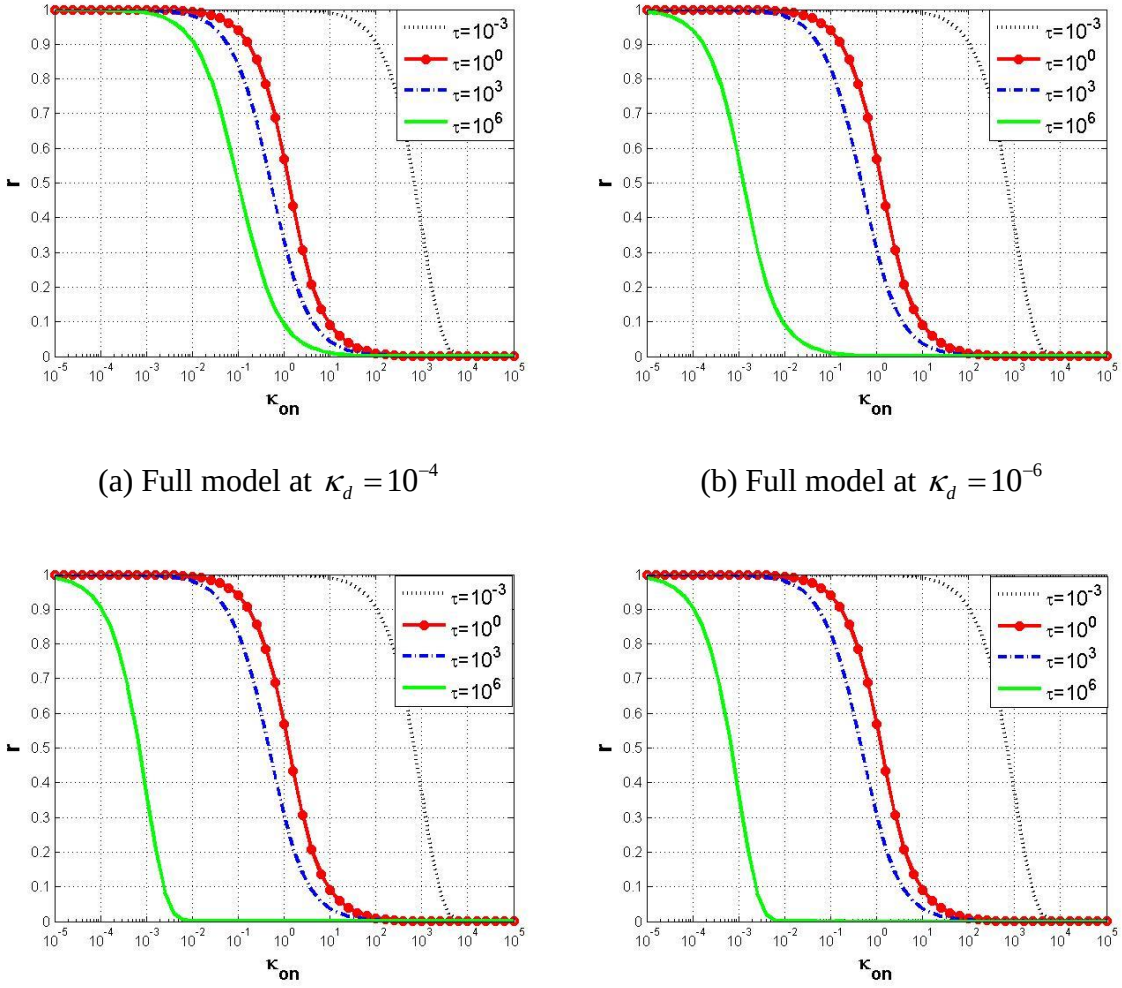

(a) Full model at $\kappa_d = 10^{-4}$ (b) Full model at $\kappa_d = 10^{-6}$

(c) Full model at $\kappa_d = 10^{-8}$ (d) Simplified model (12)

Fig. 2 Dose response curves predicted for four different incubation times, when $\kappa_i = 0.001$. Incubation times shown in the figure legend: black dotted line for 10^{-3}; red line with circles for 10^{0}; blue dash-dot line for 10^{3}; green solid line for 10^{6}. (a) Full model (9) simulated at $\kappa_d = 10^{-4}$; (b) Full model simulated at $\kappa_d = 10^{-6}$; (c) Full model simulated at $\kappa_d = 10^{-8}$; (d) Approximate model in (12).

The approximate model in (12) represents a homogeneous LTI system with $\mathbf{A} = \begin{bmatrix} -\kappa_{on} & 1 \\ \kappa_{on} & -(1+\kappa_i) \end{bmatrix}$. We can use the eigenvalue method to analyse its dynamic characteristics. Denoting the trace and determinant of matrix **A** as

$T = \text{trace}(\mathbf{A}) = -\left(1+\kappa_{on}+\kappa_i\right)$, $\Delta = \det(\mathbf{A}) = \kappa_{on}\cdot\kappa_i$, the eigenvalues of $\mathbf{A}$ are calculated by $\lambda_{1,2} = \left(T \mp \sqrt{T^2 - 4\Delta}\right)\Big/2$.

For the first eigenvalue

$$\lambda_1 = -\frac{1}{2}\left(1+\kappa_{on}+\kappa_i\right) - \frac{1}{2}\sqrt{\left(1+\kappa_{on}+\kappa_i\right)^2 - 4\kappa_{on}\kappa_i}, \tag{14}$$

its associated eigenvector is

$$v_1 = \begin{bmatrix} v_{11} & v_{21} \end{bmatrix}^{\mathrm{T}} = \begin{bmatrix} \dfrac{1+\kappa_i-\kappa_{on}-\sqrt{\left(1+\kappa_{on}+\kappa_i\right)^2 - 4\kappa_{on}\kappa_i}}{2\kappa_{on}} & 1 \end{bmatrix}^{\mathrm{T}}. \tag{15}$$

For the second eigenvalue

$$\lambda_2 = -\frac{1}{2}\left(1+\kappa_{on}+\kappa_i\right) + \frac{1}{2}\sqrt{\left(1+\kappa_{on}+\kappa_i\right)^2 - 4\kappa_{on}\kappa_i}, \tag{16}$$

its associated eigenvector is

$$v_2 = \begin{bmatrix} v_{12} & v_{22} \end{bmatrix}^{\mathrm{T}} = \begin{bmatrix} \dfrac{1+\kappa_i-\kappa_{on}+\sqrt{\left(1+\kappa_{on}+\kappa_i\right)^2 - 4\kappa_{on}\kappa_i}}{2\kappa_{on}} & 1 \end{bmatrix}^{\mathrm{T}}. \tag{17}$$

With initial conditions $r_0 = 1$ and $c_0 = 0$, a general analytical solution for (12) can be succinctly written as

$$\mathbf{M}(\tau) = \begin{bmatrix} r(\tau) \\ c(\tau) \end{bmatrix} = \frac{1}{v_{11}-v_{12}} \begin{bmatrix} v_{11}e^{\lambda_1\tau} - v_{12}e^{\lambda_2\tau} \\ e^{\lambda_1\tau} - e^{\lambda_2\tau} \end{bmatrix} \tag{18}$$

where all terms regarding eigenvalues and entries in eigenvectors are provided in (14) - (17).

The $\log_{10}$ transformed ratio of the two eigenvalues for different pairs of (κ_{on}, κ_i) is plotted in a heat map as shown in Fig. 3. From this diagram it is evident that when the two parameters have similar values and are both above 1, the two eigenvalues λ_1 and λ_2 are close to each other (the red area in Fig. 3). However, if only one parameter is much larger than 1 or both parameters are much smaller than 1, then the two eigenvalues are widely apart from each other, i.e. $\lambda_2 / \lambda_1 \ll 1$ (the blue area in Fig. 3), and the time response of the system is mainly determined by $|\lambda_1|$ in a shorter period.

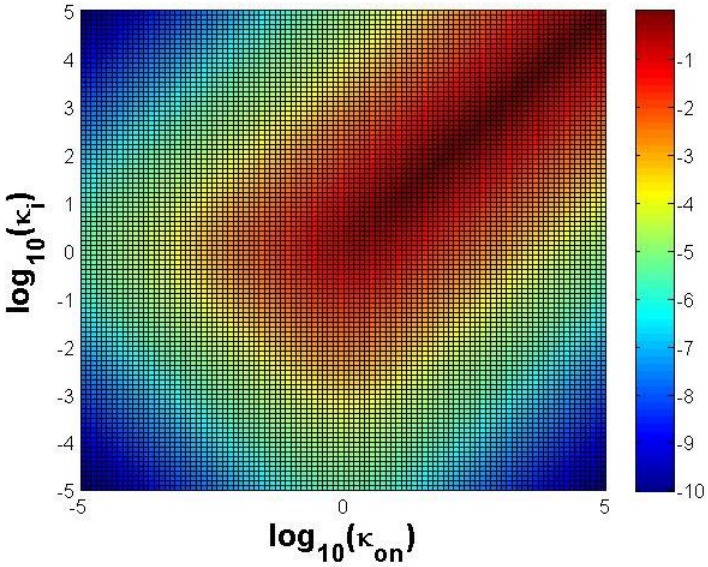

Fig. 3 $\log_{10}(\lambda_2 / \lambda_1)$ plotted as a function of $\log_{10}(\kappa_{on})$ and $\log_{10}(\kappa_i)$. Values between -10 and 0 are colour-coded.

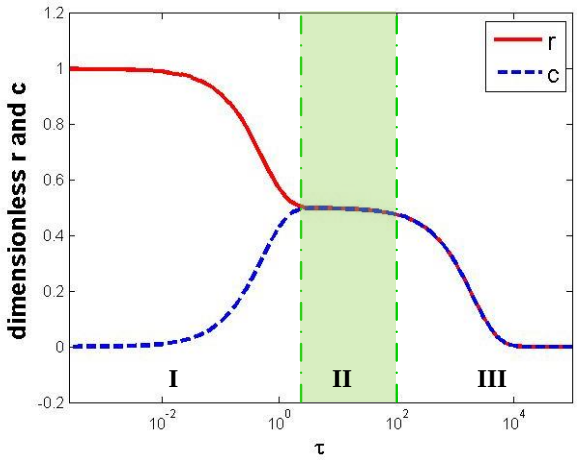

Fig. 4 Time responses of *r* and *c* under $\kappa_{on} = 1$, $\kappa_i = 0.001$ and $\kappa_d = 0$.

For example, when $\kappa_{on} = 1$, $\kappa_i = 0.001$, from (14) to (17), the eigenvalues and eigenvectors can be calculated as: $\lambda_1 = -2.005$, $\lambda_2 = -5\times10^{-4}$, $\nu_1 = \begin{bmatrix}-0.7069 & 0.7069\end{bmatrix}^{\mathrm{T}}$ and $\nu_2 = \begin{bmatrix}-0.7073 & -0.7069\end{bmatrix}^{\mathrm{T}}$. The short-term time response is driven by $|\lambda_1|$ (see region I in Fig. 4), and the long-term time response is driven by $|\lambda_2|$ (see region III in Fig. 4). Interestingly, between these two regions, both *r* and *c* have relatively small variations (see region II in Fig. 4). Hence, corresponding dose responses simulated for observation times in this shadowed region would appear to be similar using experimental data. This time-independent observation may suggest a reversible inhibition, which is not true from the above analysis.

3.2 Fast drug binding/dissociation and fast covalent modification

The parametric regime for this scenario is classified by: $\kappa_{on} \gg \kappa_d$, $\kappa_{off} \gg \kappa_d$, and $\kappa_i \approx \kappa_{on}$, therefore $\kappa_i \gg \kappa_d$. In this case, both reversible binding/dissociation and irreversible modification are much faster than receptor turnover. The system can also be modelled by (12). It can be seen from the heat map in Fig. 3 that the two eigenvalues are close to each other in this region, which means the two inherent time scales are not far away from each other. For the simulations demonstrated in Fig. 5, the two eigenvalues are $\lambda_1 = -2.618$ and $\lambda_2 = -0.382$, calculated from (14) and (16), respectively. In this case, the dose response curves measured at different incubation times are predicted to be clearly separated from each other (Fig. 5 (a)).

The concentrations of R and C reach steady states with both values at 0 (Fig. 5 (b)), which is consistent with the steady-state analysis conclusion given in (13). Similar to the simulation results shown in Fig. 4, Fig. 5 (b) also demonstrates that the receptor concentration decreases monotonically to its steady state, but the complex concentration goes through a rapid increase initially and then decreases in a slower time scale to its steady state.

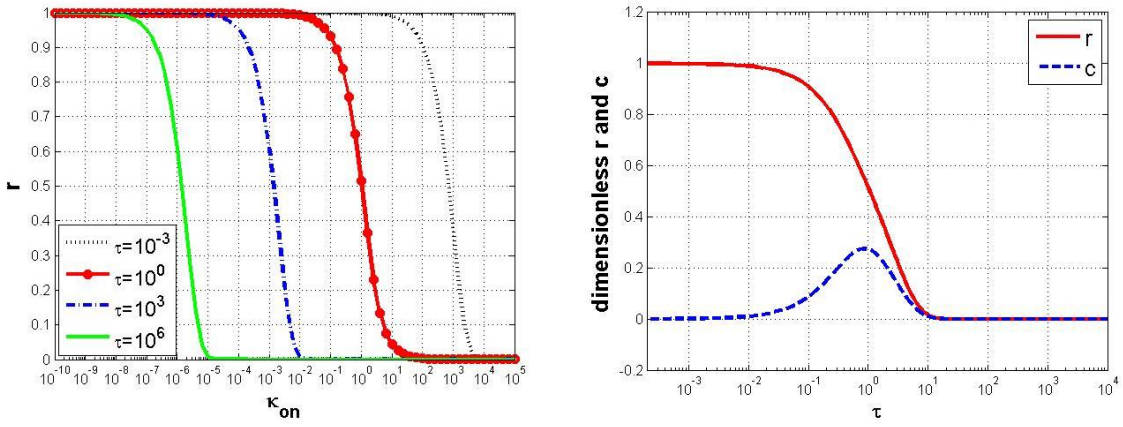

(a) Dose response curves (b) Time responses under $\kappa_{on} = 1$

Fig. 5 Dose response curves and time responses of *r* and *c* under $\kappa_d = 0$, $\kappa_{on} = \kappa_i = 1$.

3.3 Fast drug binding/dissociation and slow covalent modification

Under the condition of fast drug process over receptor turnover ($k_{off} \gg k_d$ and $k_{on} \gg k_d$), we further consider the regime of $k_{off} \gg k_i$, i.e., $\kappa_i \ll 1$. This means the drug dissociation is much faster than the covalent modification. It corresponds to the region in lower part of the heat map in Fig. 3. This condition is satisfied if i) an irreversible inhibitor has to overcome a

relatively large energy barrier to covalently modify the receptor; ii) drug dissociation is rapid; iii) a combination of both. Within the parametric region of $\kappa_{on} \gg \kappa_d$, $\kappa_d \ll 1$ and $\kappa_i \ll 1$, model (12) can be further reduced to

$$\begin{bmatrix} \dot{r} \\ \dot{c} \end{bmatrix} = \begin{bmatrix} -\kappa_{on} & 1 \\ \kappa_{on} & -1 \end{bmatrix} \begin{bmatrix} r \\ c \end{bmatrix} \tag{19}$$

Model (19) is a description for protein-based assay when reversible inhibitor is applied while the covalent modification is negligible. In order to determine how small κ_i should be so that the simplified model in (19) can be applied, simulations are conducted using the full model under $\kappa_d = 10^{-8}$, and reduce κ_i gradually to search for the threshold level that will produce a response close to the simplified model response. Fig. 6 shows that when κ_i is reduced to 1×10^{-7}, the full-model response is very close to that of the simplified model (19). This suggests that when $\kappa_i \le 10^{-7}$, the simplified model in (19) can be used to approximate model (12) with a good accuracy.

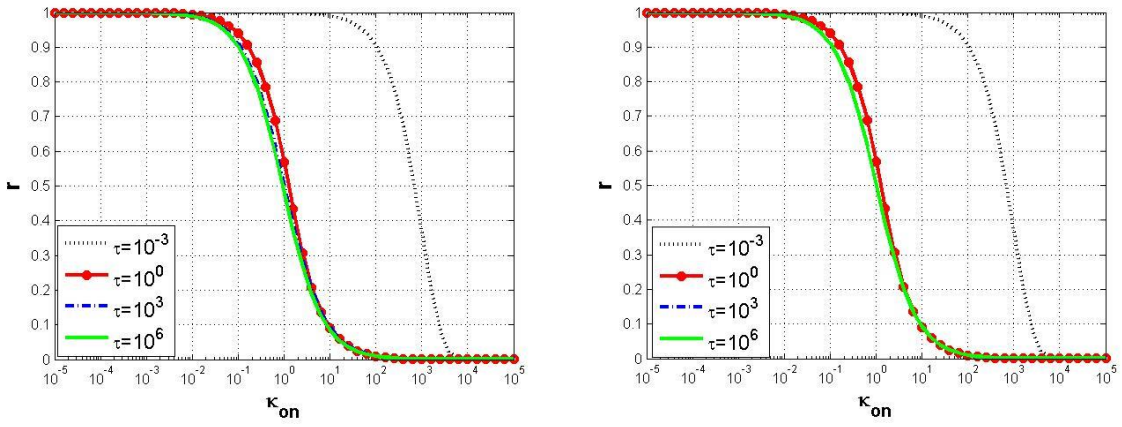

(a) Full model at $\kappa_d = 1\times10^{-8}, \kappa_i = 1\times10^{-7}$ (b) Approximate model (19)

Fig. 6 Dose response curves predicted for different incubation times in τ: black dotted line for 10^{-3}; red line with circles for 10^{0}; blue dash-dot line for 10^{3}; green solid line for 10^{6}. (a) Full model (9) simulated at $\kappa_d = 1\times10^{-8}, \kappa_i = 1\times10^{-7}$; (b) Approximate model in (19).

In this case, $\dfrac{\mathrm{d}r}{\mathrm{d}\tau} = -\dfrac{\mathrm{d}c}{\mathrm{d}\tau}$, $T = \mathrm{trace}(\mathbf{A}) = -(1+\kappa_{on})$, $\Delta = \det(\mathbf{A}) = 0$, $\lambda_1 = T = -(\kappa_{on}+1)$ and $\lambda_2 = 0$. Under the given initial conditions, the time responses of the two dimensionless concentration terms can be solved explicitly to yield

$$r(\tau)=\frac{1}{1+\kappa_{on}}\left(1+\kappa_{on}e^{-(1+\kappa_{on})\tau}\right)$$
$$c(\tau)=\frac{\kappa_{on}}{1+\kappa_{on}}\left(1-e^{-(1+\kappa_{on})\tau}\right) \tag{20}$$

The time scale of this dynamic system is determined by $|\lambda_1|$ or by κ_{on}. The larger is κ_{on}, the faster response the system has, and vice versa. The time responses of r and c under different levels of κ_{on} are illustrated in Fig. 7.

With model (19), the steady state is not determined by (13) since κ_i is taken to be zero. In fact, the equilibrium points for system (19) can be derived from (20) to give

$$r_{ss}=\lim_{\tau\to\infty}\frac{1}{1+\kappa_{on}}\left(1+\kappa_{on}e^{-(1+\kappa_{on})\tau}\right)=\frac{1}{1+\kappa_{on}}$$
$$c_{ss}=\lim_{\tau\to\infty}\frac{\kappa_{on}}{1+\kappa_{on}}\left(1-e^{-(1+\kappa_{on})\tau}\right)=\frac{\kappa_{on}}{1+\kappa_{on}} \tag{21}$$

It can be concluded that $r_{ss}+c_{ss}=1$ at the steady state. The larger is κ_{on}, the smaller is r_{ss} and the larger is c_{ss}. This can be clearly seen in the dynamic simulation results shown in Fig. 7.

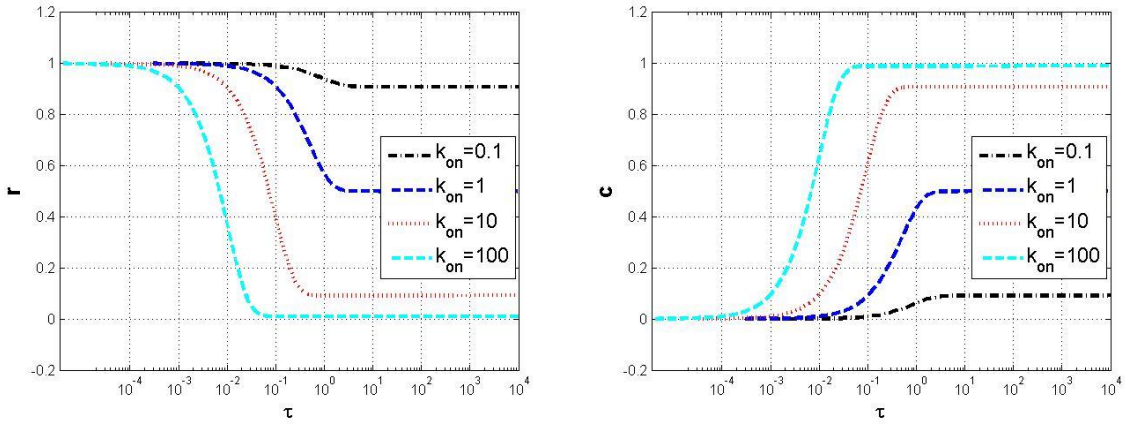

(a) Time response r (b) Time response c

Fig. 7 Time responses of r and c with approximate model (19) under different levels of κ_{on}.

For incubation time $\tau_m \gg 1/(1+\kappa_{on})$, r is close to its steady state (see simulation for each κ_{on} in Fig. 7). Hence, dose response measurements taken beyond this point would appear time-invariant.

In summary, our analysis of fast drug process suggests for dose response to appear time-invariant, the following two requirements need to be satisfied. Firstly, the apparent first-order rate κ_{on} and the first-order covalent bond formation rate κ_i need to be largely different so that the two time scales characterized by $1/|\lambda_1|$ and $1/|\lambda_2|$ are well separated from each other. Secondly, observation time has to be between the two time scales, which corresponds to region II in Fig. 4. It can also be observed from dynamic study that the receptor concentration always decreases monotonically to a steady-state level of zero for the fast drug process, while the concentration of complex C increases rapidly first and then decreases gradually to zero except for the case when covalent modification to complex C is negligible, i.e. $\kappa_i = 0$.

4 Slow drug process relative to receptor turnover

In the parametric regime where $k_{off} \approx k_d$ or $k_{off} \ll k_d$, i.e. $\kappa_d \approx 1$ or $\kappa_d \gg 1$, target coverage duration is comparable to or longer than the receptor life time. This can happen due to: i) long period of target coverage; ii) fast receptor degradation; and iii) combination of both. This might be biologically relevant when receptor homeostasis is tightly regulated at the turnover level. The full model in (9) is used in this regime.

Again the eigenvalue method can be used to analyze the system dynamics. The homogeneous part of (9) is $\dot{\mathbf{X}} = \mathbf{A}\mathbf{X}$. The trace of $\mathbf{A}$ is $T = \text{trace}(\mathbf{A}) = -\left(1 + \kappa_{on} + \kappa_d + \kappa_i\right)$, the determinant of $\mathbf{A}$ is $\Delta = \det(\mathbf{A}) = \kappa_d + \kappa_{on}\kappa_i + \kappa_d\kappa_i$. The two eigenvalues are $\lambda_{1,2} = \frac{1}{2}\left(T \mp \sqrt{T^2 - 4\Delta}\right)$.

For $\lambda_1 = \frac{1}{2}\left(T - \sqrt{T^2 - 4\Delta}\right)$, the associated eigenvector is

$$v_1 = \begin{bmatrix} v_{11} & v_{21} \end{bmatrix}^{\mathrm{T}} = \left[\frac{1 + \kappa_i - \left(\kappa_{on} + \kappa_d\right) - \sqrt{\left(1 + \kappa_i - \kappa_{on} - \kappa_d\right)^2 + 4\kappa_{on}}}{2\kappa_{on}} \quad 1 \right]^{\mathrm{T}}.$$

For $\lambda_2 = \frac{1}{2}\left(T + \sqrt{T^2 - 4\Delta}\right)$, the associated eigenvector is

$$v_2 = \begin{bmatrix} v_{12} & v_{22} \end{bmatrix}^{\mathrm{T}} = \left[\frac{1 + \kappa_i - \left(\kappa_{on} + \kappa_d\right) + \sqrt{\left(1 + \kappa_i - \kappa_{on} - \kappa_d\right)^2 + 4\kappa_{on}}}{2\kappa_{on}} \quad 1 \right]^{\mathrm{T}}.$$

Under the initial condition of $\mathbf{X}_0 = \begin{bmatrix} 1 & 0 \end{bmatrix}^{\mathrm{T}}$, the general solution to the homogeneous part can be written as $\mathbf{M}(\tau)$ in (18). Taking the non-homogeneous part $\mathbf{f} = \begin{bmatrix} \kappa_d & 0 \end{bmatrix}^{\mathrm{T}}$ into account, the general solution to (9) is written as follows

$$\begin{bmatrix} r(\tau) & c(\tau) \end{bmatrix}^{\mathrm{T}} = \mathbf{M}(\tau)\mathbf{M}(0)^{-1}\mathbf{X}_0 + \mathbf{M}(\tau)\int_0^{\tau} \mathbf{M}(t)^{-1}\mathbf{f}(t)\,\mathrm{d}t \tag{22}$$

The steady-state values of *r* and *c* can be obtained through numerical integration with (22), or calculated explicitly by (10) and (11).

Similar to the heat map in Fig. 3, we first plot $\log_{10}(\lambda_2 / \lambda_1)$ as a function of κ_{on} and κ_i in $\log_{10}$ scales (Fig. 8). Taking $k_{off} = k_d$, i.e. $\kappa_d = 1$ (Fig. 8 (a)), separation of time scales happens if either $k_{on} \gg k_{off}$ and $k_i \ll k_{off}$ (blue region in Fig. 8 (a)), or $k_{on} \ll k_{off}$ and $k_i \gg k_{off}$ (light green region in Fig. 8 (a)), with the former leads to more pronounced effects. In contrast, in the case of $k_{off} = 0.001 k_d$, i.e. $\kappa_d = 1000$ (Fig. 8 (b)), separation of time scales takes place if $k_i \ll k_{off}$ (bottom part in Fig. 8 (b)), and the condition of $k_{on} \gg k_{off}$ makes the separation more pronounced.

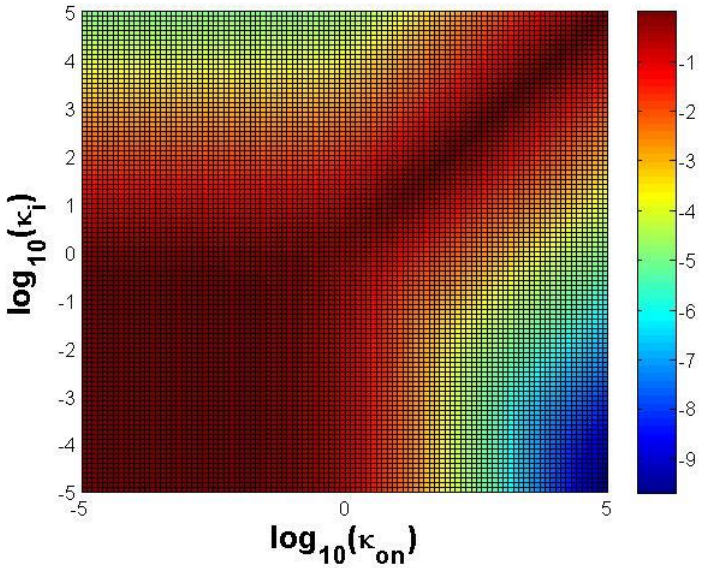

(a) $k_{off} = k_d$

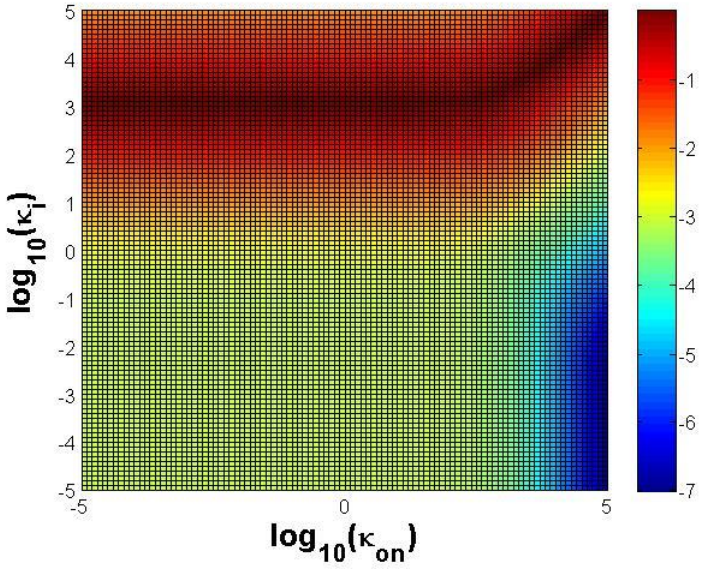

(b) $k_{off} = 0.001k_d$

Fig. 8 $\log_{10}(\lambda_2 / \lambda_1)$ plotted as a function of $\log_{10}(\kappa_{on})$ and $\log_{10}(\kappa_i)$. Values between -10 and 0 are colour-coded. (a) $k_{off} = k_d$; (b) $k_{off} = 0.001k_d$.

The following can be verified in this parametric regime: $-v_{11}\lambda_2(\kappa_d + \lambda_1) < 0$, $v_{12}\lambda_1(\kappa_d + \lambda_2) > 0$. Considering the analytic solution, it is likely for *r* to decrease first with a time scale determined by $|\lambda_1|$ and then recover with a time scale determined by $|\lambda_2|$ in the longer term, if $|\lambda_1|$ and $|\lambda_2|$ are sufficiently apart.

An example is discussed to illustrate these ideas by taking $k_{off} = k_d$ and $k_i \ll k_d$. This means the receptor degradation is as fast as target coverage and the drug overcomes a large energy barrier to covalently modify the receptor.

Suppose $k_{off} = k_d$ and $k_i = 0.001k_d$. Under this condition, receptor initially decreases as a result of drug inhibition, and then recovers towards steady states (see Fig. 9 (c) and Fig. 9 (d)). In the context of dose response curves, this means measurement taken before recovery in *r* would make the drug appear more potent than the actual steady-state response. For $\kappa_{on} = 1$, *r* is predicted to be smaller for $\tau = 1$ than for $\tau = 10, 100, 1000$ (Fig. 9 (a)). In addition, this trend is consistent throughout κ_{on} values to a larger range (Fig. 9 (b)). Hence, the dose response simulated for $\tau = 1$ (black dotted curve) appears to be more potent than any other curves in Fig. 9 (a)-(b).

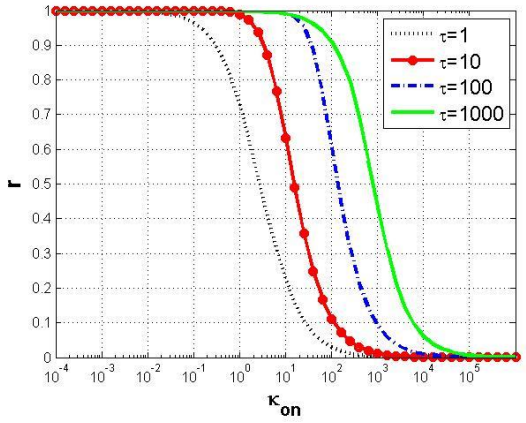

(a) $\tau = [1, 10^3]$

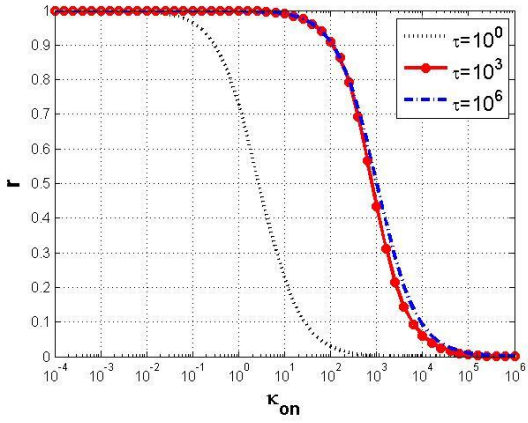

(b) $\tau = [1, 10^6]$

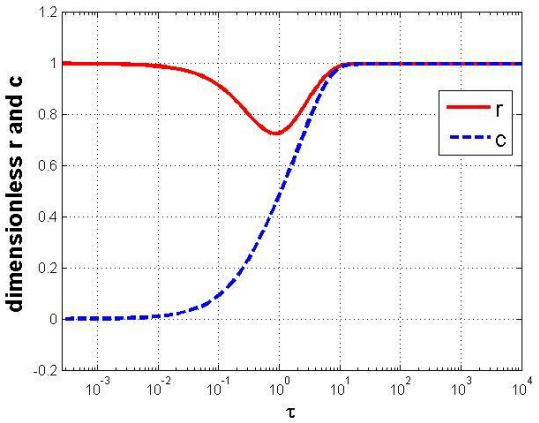

(c) $\kappa_{on} = \kappa_d = 1$

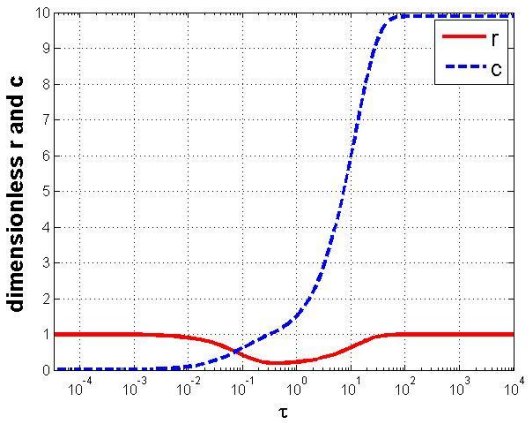

(d) $\kappa_{on} = 10, \kappa_d = 1$

Fig. 9 Dose response curves, time response of *r* and *c* under $\kappa_i = 0.001$.

According to the heat map in Fig. 8 (a), higher κ_{on} leads to smaller λ_2 (the blue region in Fig. 8 (a)), which makes recovery time in *r* being longer. To examine this observation, time responses of *r* and *c* are simulated for $\kappa_{on} = 1$ and $\kappa_{on} = 10$, respectively, as shown in Fig. 9 (c) and (d). It can be seen that time response simulation at $\kappa_{on} = 10$ predicts an elongated recovery period in *r* (Fig. 9 (d)) compared with that in $\kappa_{on} = 1$ (Fig. 9 (c)). This observation is consistent with the separation of different dose response curves in Fig. 9 (a).

In slow drug process, the increase of complex concentration is monotonic over time, while the receptor concentration first decreases in a short time and then increase towards a constant level in a longer time. The numerical solutions for *r* and *c* at steady states shown in Fig. 9 (c) and (d) are validated by the model-based analytical results in (10) and (11).

5 Applications

Aberrant activity in Epidermal Growth Factor Receptor (EGFR) signaling has profound implications in different types of tumour. Recently, k_{off}/k_{on} and k_i are reliably quantified from cell-free assays for different irreversible EGFR mutant (EGFRm) inhibitors [20]. However, this study was not able to determine the actual values of $\kappa_{on} = k_{on}^{*}[afatinib]/k_{off}$ and k_{off}. Instead, k_{on}^{*}, that is $k_{on}/[\text{drug}]$ in our context, was assumed to be close to diffusion limit at $100\mu M^{-1}s^{-1}$ in order to calculate values for k_{off}. The reported values are tabulated below:

compound	k_{off}, s^{-1}	k_i, s^{-1}	Ki(nM)
CI-1033	0.19±0.04	0.011±0.0002	1.9±0.4
dacomitinib	1.1±0.1	0.0018±0.0001	10.7±0.9
afatinib	0.3±0.1	0.0024±0.0003	2.8±0.6
neratinib	0.2±0.1	0.0011±0.0002	2.4±0.5
CL-387785	18±4	0.002±0.0003	180±40
WZ-4002	23±5	0.0049±0.0015	230±50

Table 1. Parameter values inferred from reaction progress curves measured for H1975 cells carrying L858R and T790M mutations in EGFR, using an ODE model. This table is reproduced from the supplementary information in [20]. The plus-or-minus values are standard deviations from averaging three replicated, entirely independent experiments. $K_i = k_{on}/k_{off}$.

We simulated the cell-free assay of afatinib by using the model in (9) by taking $\kappa_d = 0$. This predicts the IC_{50} for κ_{on} at 30-minutes incubation has a mean value of 0.13 (i.e. assuming $k_i = 2.4\times10^{-3}s^{-1}$, $k_{off} = 0.3s^{-1}$) (see Fig. 10 (a)). Since $\kappa_{on} = k_{on}^{*}[afatinib]/k_{off}$, afatinib's IC_{50} at 30-minutes incubation is predicted to be 0.4nM. Considering different combinations of k_i and k_{off} values as reported in Table 1, afatinib's IC_{50} at 30-minute incubation is predicted to be within the range of [0.27,0.6] nM.

It is reported that the internalisation rate of EGFR receptor is approximately 0.2min^{-1} in breast cancer cells [21]. Hence, $\kappa_d = k_d / k_{off} = 1.1\times10^{-2}$. Considering $\kappa_i = 8.0\times10^{-3}$, this is similar to the fast drug process parametric regime discussed in Section 3.3. Model simulation in Fig. 6 suggests dose response curves taken at $\tau = 1$ and $\tau = 100$ should be close.

Using model (12) to mimic *in vitro* cell assay conditions by taking $\kappa_d = 1.1\times10^{-2}$, simulated dose response curves at different incubation durations shift further to right (Fig. 10 (b)) compared with that of $\kappa_d = 0$ (Fig. 10 (a)). In Fig. 10 (b), with IC_{50} for κ_{on} at 1-hour incubation at approximately 1.4, a 10-fold increase from the predicted protein-based assay (i.e. 0.13) is observed. Consistent with these simulation results, approximately 10-fold difference was reported for cell-based assay and protein-based assay for afatinib [21]

It can be seen from the above discussions that the simple model in (9) can be used conveniently to generate insights into the connections and differences between protein-based assay and cell-based assay.

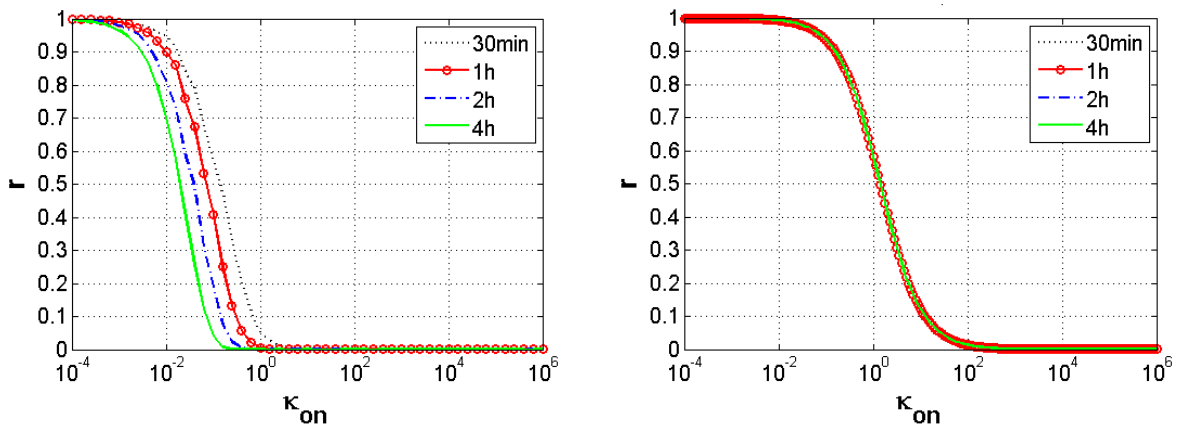

(a) $\kappa_d = 0$, $\kappa_i = 8.0\times10^{-3}$. This mimics the cell-free assay condition.

(b) $\kappa_d = 1.1\times10^{-2}$, $\kappa_i = 8.0\times10^{-3}$. This mimics the *in vitro* cell assay.

Fig. 10 Simulated dose response curves for *afatinib*.

6. Conclusions and discussions

At lead generation and optimization, it is important to understand the Mechanism Of Action (MOA) of a chemical compound, as well as the Structure-Activity Relationship (SAR), in the hope that ultimately a compound with sufficient therapeutic efficacy is taken further for preclinical development. Reversibility of a compound is a crucial aspect of MOA

characterisation. This often remains unknown for compounds coming out of empirical screening methods. Towards this goal, assays have been established to study inhibition reversibility [22]. It is generally accepted that response to irreversible inhibitors are time-dependent. Hence, it is often taken for granted that time-independence indicates inhibition reversibility. However, our model-based analysis refutes this claim.

We demonstrated iff inhibitor binding and dissociation processes are much quicker than receptor turnover, this system can be approximated by one concerning inhibition only, which is equivalent to the protein-based assay. Based on the numerical simulation using a simple model, it is observed that for protein-based assays, under certain parameter conditions, the dose response curves can be very similar to each other (compare the middle curves in Fig. 2 (d)), given 1000-fold variation in incubation time. This indicates dose responses might appear time-invariant for a particular parameter setting. In practice, these data might not be statistically different and can be erroneously taken as evidence of reversible inhibitor.

We subsequently analyzed the impact of cell parameters on dose response, including target synthesis and degradation, using the proposed model. Our ensuing analysis of the eigenvalues provides a more general understanding. For dose response to appear time-invariant, the apparent first-order association rate κ_{on} and the first-order covalent bond formation rate κ_i need to be well separated so that the system has two very different time scales. In particular, when a slowly-dissociating irreversible drug is applied to a receptor under fast turnover, dose response may be highly similar to each other under a variety of incubation periods. Hence, it is inappropriate to conclude an inhibitor being reversible given time-independent dose response, either based on protein-based assay or cell-based assay.

The main purpose of this analysis is to demonstrate the relationship between dose response and parameter values in drug and cell processes. For the sake of simplicity, we only considered a linear model in which each reaction follows first-order kinetics. In addition, we did not consider biological regulation over synthesis, degradation and sub-cellular localisation of a receptor [20]. Results obtained in this paper are specific to the form of this linear model. In reality, receptors are often regulated under different levels via feedback mechanisms. This often necessitates mechanistic modelling of a biological pathway to aid in interpretation of *in vitro* cell assays.

It is evident from both numerical simulation and analytical study that the proposed model is globally asymptotically stable. For the fast drug process considering complex elimination,

the reduced model (12) is proposed. The receptor concentration decreases monotonically to its steady-state level of zero, while the complex concentration initially increases rapidly and then decreases gradually to zero when the complex elimination is considered (see (13) for steady-state calculation). When the complex elimination is negligible, the reduced model (19) is used. The system will have non-zero steady states for both *r* and *c* following a conservation law of $r_{ss} + c_{ss} = 1$ (see (21) for the explicit solution). For the slow drug process including both reactions (1) and (2), the full model (9) is used to describe the dynamic system, and the steady-states are explicitly represented by (10) and (11) for *r* and *c*, respectively. In this case, the complex concentration increases monotonically over the whole process, but the receptor concentration first decreases rapidly and then increases gradually on a slower time scale back towards its steady state. The similar rebound behaviour in receptor was also observed and discussed in other TMDD model-based studies [12; 14; 15].

For a drug discovery and development programme, the *in vitro* model should be used to identify parameter values from *in vitro* data. These parameters can be used subsequently to help identify the remaining parameter values in the *in vivo* model. This step-wise fitting may reduce uncertainty in parameter estimation. In this context, the *in vitro* model described in this paper improves the utility of TMDD models.

Acknowledgment

TY would gratefully acknowledge Hitesh Mistry (University of Manchester), James Yates (AstraZeneca UK Ltd) and Chris Brackley (University of Edinburgh) for useful discussions. HY would like to thank Professor Peter Halling and Mr Hui Yu from the University of Strathclyde for useful discussions and support in Matlab coding.

References

[1] Sorger, P. K., Allerheiligen, S. R., Abernethy, D. R., *et al.*: 'Quantitative and systems pharmacology in the post-genomic era: new approaches to discovering drugs and understanding therapeutic mechanisms', NIH Bethesda, An NIH white paper by the QSP workshop group, 2011), 1-48

[2] Gibiansky, L. and Gibiansky, E.: 'Target-mediated drug disposition model: approximations, identifiability of model parameters and applications to the population pharmacokinetic and pharmacodynamic modeling of biologics', *Expert Opin Drug Metab Toxicol,* 2009, **5**, (7), 803-812

[3] Ma, P.: 'Theoretical considerations of target-mediated drug disposition models: simplifications and approximations', *Pharmaceutical research*, 2012, **29**, (3), 866-882

[4] Marathe, A., Krzyzanski, W. and Mager, D. E.: 'Numerical validation and properties of a rapid binding approximation of a target-mediated drug disposition pharmacokinetic model', *Journal of Pharmacokinetics and Pharmacodynamics*, 2009, **36**, (3), 199-219

[5] Yan, X., Mager, D. E. and Krzyzanski, W.: 'Selection between Michaelis–Menten and target-mediated drug disposition pharmacokinetic models', *Journal of pharmacokinetics and pharmacodynamics*, 2010, **37**, (1), 25-47

[6] Vicini, P.: 'Multiscale modeling in drug discovery and development: future opportunities and present challenges', *Clinical Pharmacology & Therapeutics*, 2010, **88**, (1), 126-129

[7] Mager, D. E. and Krzyzanski, W.: 'Quasi-equilibrium pharmacokinetic model for drugs exhibiting target-mediated drug disposition', *Pharmaceutical Research*, 2005, **22**, (10), 1589-1596

[8] Gibiansky, L. and Gibiansky, E.: 'Target-mediated drug disposition model: relationships with indirect response models and application to population PK–PD analysis', *Journal of Pharmacokinetics and Pharmacodynamics*, 2009, **36**, (4), 341-351

[9] Orrell, D. and Fernandez, E.: 'Using predictive mathematical models to optimise the scheduling of anti-cancer drugs', *Innovations in Pharmaceutical Technology*, 2010, **33**, 58-62

[10] Yankeelov, T. E., Atuegwu, N., Hormuth, D., *et al.*: 'Clinically relevant modeling of tumor growth and treatment response', *Science Translational Medicine*, 2013, **5**, (187), 187ps9-187ps9

[11] Bonate, P.: 'What happened to the modeling and simulation revolution?', *Clinical Pharmacology & Therapeutics*, 2014, **96**, (4), 416-417

[12] Aston, P. J., Derks, G., Agoram, B. M. and Van Der Graaf, P. H.: 'A mathematical analysis of rebound in a target-mediated drug disposition model: I. Without feedback', *Journal of Mathematical Biology*, 2014, **68**, (6), 1453-1478

[13] Peletier, L. A. and Gabrielsson, J.: 'Dynamics of target-mediated drug disposition', *European Journal of Pharmaceutical Sciences*, 2009, **38**, (5), 445-464

[14] Peletier, L. A. and Gabrielsson, J.: 'Dynamics of target-mediated drug disposition: characteristic profiles and parameter identification', *Journal of Pharmacokinetics and Pharmacodynamics*, 2012, **39**, (5), 429-451

[15] Aston, P. J., Derks, G., Raji, A., Agoram, B. M. and Van Der Graaf, P. H.: 'Mathematical analysis of the pharmacokinetic–pharmacodynamic (PKPD) behaviour

of monoclonal antibodies: predicting in vivo potency', *Journal of theoretical biology*, 2011, **281**, (1), 113-121

[16] Strelow, J., Dewe, W., Iversen, P., *et al.*: 'Mechanism of Action assays for Enzymes', 2004,

[17] Nagar, S., Jones, J. P. and Korzekwa, K.: 'A numerical method for analysis of in vitro time-dependent inhibition aata. Part 1. theoretical considerations', *Drug Metabolism and Disposition*, 2014, **42**, (9), 1575-1586

[18] Copeland, R. A., Pompliano, D. L. and Meek, T. D.: 'Drug–target residence time and its implications for lead optimization', *Nature Reviews Drug Discovery*, 2006, **5**, (9), 730-739

[19] You, T., Stansfield, I., Romano, M. C., Brown, A. J. and Coghill, G. M.: 'Analysing GCN4 translational control in yeast by stochastic chemical kinetics modelling and simulation', *BMC systems biology*, 2011, **5**, (1), 131

[20] Lauffenburger, D. A. and Linderman, J. J. *Receptors: models for binding, trafficking, and signaling*. Oxford University Press New York:, 1993.

[21] Hendriks, B. S., Opresko, L. K., Wiley, H. S. and Lauffenburger, D.: 'Coregulation of Epidermal Growth Factor Receptor/Human Epidermal Growth Factor Receptor 2 (HER2) Levels and Locations Quantitative Analysis of HER2 Overexpression Effects', *Cancer Research*, 2003, **63**, (5), 1130-1137

[22] Schwartz, P. A., Kuzmic, P., Solowiej, J., *et al.*: 'Covalent EGFR inhibitor analysis reveals importance of reversible interactions to potency and mechanisms of drug resistance', *Proceedings of the National Academy of Sciences*, 2014, **111**, (1), 173-178